The Astrophysical Journal, 954:3 (15pp), 2023 September 1 https://doi.org/10.3847/1538-4357/ace523


# Discovery of the Elusive Carbonic Acid (HOCOOH) in Space

Miguel Sanz-Novo[1,2], Víctor M. Rivilla[1], Izaskun Jiménez-Serra[1], Jesús Martín-Pintado[1], Laura Colzi[1], Shaoshan Zeng[3], Andrés Megías[1], Álvaro López-Gallifa[1], Antonio Martínez-Henares[1], Sarah Massalkhi[1], Belén Tercero[4], Pablo de Vicente[5], Sergio Martín[6,7], David San Andrés[1], and Miguel A. Requena-Torres[8,9]
[1] Centro de Astrobiología (CAB), INTA-CSIC, Carretera de Ajalvir km 4, Torrejón de Ardoz, E-28850 Madrid, Spain
[2] Computational Chemistry Group, Departamento de Química Física y Química Inorgánica, Universidad de Valladolid, E-47011 Valladolid, Spain
[3] Star and Planet Formation Laboratory, Cluster for Pioneering Research, RIKEN, 2-1 Hirosawa, Wako, Saitama, 351-0198, Japan
[4] Observatorio Astronómico Nacional (OAN-IGN), Calle Alfonso XII, 3, E-28014 Madrid, Spain
[5] Observatorio de Yebes (OY-IGN), Cerro de la Palera SN, Yebes, Guadalajara, Spain
[6] European Southern Observatory, Alonso de Córdova 3107, Vitacura 763 0355, Santiago, Chile
[7] Joint ALMA Observatory, Alonso de Córdova 3107, Vitacura 763 0355, Santiago, Chile
[8] University of Maryland, College Park, MD 20742-2421, USA
[9] Department of Physics, Astronomy and Geosciences, Towson University, Towson, MD 21252, USA
*Received 2023 June 10; revised 2023 July 5; accepted 2023 July 5; published 2023 August 18*

## Abstract

A quarter century after the detection of the last interstellar carboxylic acid, acetic acid ($CH_3COOH$), we report the discovery of a new one, the *cis-trans* form of carbonic acid (HOCOOH), toward the Galactic center molecular cloud G+0.693–0.027. HOCOOH stands as the first interstellar molecule containing three oxygen atoms and the third carboxylic acid detected so far in the interstellar medium. Albeit the limited available laboratory measurements (up to 65 GHz), we have also directly identified several pairs of unblended lines in the astronomical data (between 75 and 120 GHz), which allowed us to slightly improve the set of spectroscopic constants. We derive a column density for *cis-trans* HOCOOH of $N = (6.4 \pm 0.4) \times 10^{12}$ cm$^{-2}$, which yields an abundance with respect to molecular $H_2$ of $4.7 \times 10^{-11}$. Meanwhile, the extremely low dipole moment (about 15 times lower) of the lower-energy conformer, *cis-cis* HOCOOH, precludes its detection. We obtain an upper limit to its abundance with respect to $H_2$ of $\leqslant 1.2 \times 10^{-9}$, which suggests that *cis-cis* HOCOOH might be fairly abundant in interstellar space, although it is nearly undetectable by radio astronomical observations. We derive a *cis-cis*/*cis-trans* ratio of $\leqslant 25$, consistent with the smaller energy difference between both conformers compared with the relative stability of *trans*- and *cis*-formic acid. Finally, we compare the abundance of these acids in different astronomical environments, further suggesting a relationship between the chemical content found in the interstellar medium and the chemical composition of the minor bodies of the solar system, which could be inherited during the star formation process.

*Unified Astronomy Thesaurus concepts:* Interstellar molecules (849); Interstellar clouds (834); Galactic center (565); Spectral line identification (2073); Astrochemistry (75)

*Supporting material:* FITS files

## 1. Introduction

In recent times, significant endeavors have been made to study the molecular complexity of the interstellar medium (ISM). Astronomical observations have proven that interstellar chemistry can generate diverse complex organic molecules (COMs, defined as carbon-based molecules comprised of six or more atoms; Herbst et al. 2020), highlighting several building blocks of key biomolecules (see McGuire 2022 for a recent molecular census).

Among all COMs, carboxylic acids occur widely in nature and are considered precursors of many relevant prebiotic molecules, such as amino acids and lipids (Ehrenfreund et al. 2001; Georgiou & Deamer 2014; Zhu et al. 2018). Almost 50 yr ago, Zuckerman et al. (1971) reported the detection of the first interstellar carboxylic acid, formic acid (HCOOH), in the star-forming region Sgr B2. It took more than 20 yr to detect acetic acid ($CH_3COOH$), which was also primarily identified toward Sgr B2 (Mehringer et al. 1997). Currently, both acids represent the only carboxylic acids conclusively detected in the ISM (see, e.g., Irvine et al. 1990; Remijan et al. 2003; Requena-Torres et al. 2006; Cuadrado et al. 2016; Lefloch et al. 2017; Rivilla et al. 2017; Jørgensen et al. 2018; Tercero et al. 2018; Rodríguez-Almeida et al. 2021a).

A more exotic yet well-known carboxylic acid is carbonic acid ($H_2CO_3$ or HOCOOH), a hydroxy derivative of formic acid, which appears as an auspicious astronomical candidate. This molecule plays a relevant role in various biological and geochemical processes (Loerting et al. 2000; Adamczyk et al. 2009), highlighting its implications in the global carbon cycle (Jones et al. 2014; Wang et al. 2016), in particular in the anthropogenic carbon and ocean pH (Caldeira & Wickett 2003; Ioppolo et al. 2021). Moreover, the presence of this molecule has also been suggested in different astronomical environments, such as the Galilean icy moons (Delitsky & Lane 1998; Bennett et al. 2014; Jones et al. 2014), on Mercury's north polar region (Delitsky et al. 2017), or even on the surface and/or in the atmosphere of Mars (Strazzulla et al. 1996). In fact, it has been proposed to form on the icy mantles of dust grains, which contain vast amounts of $H_2O$ and $CO_2$ (Hage et al. 1998; Moore et al. 2001; Zheng & Kaiser 2007; Oba et al. 2010; Ioppolo et al. 2021). Nevertheless, HOCOOH still awaited detection in the ISM.

Additionally, carboxylic acids are deeply ingrained in the chemical reservoir of carbonaceous chondrite meteorites

(Cooper et al. 1992; Sephton 2002; Glavin et al. 2010; Pizzarello & Shock 2010; Pizzarello et al. 2012) and comets such as 67P/Churyumov–Gerasimenko (67P/C-G; Altwegg et al. 2016), which further motivates the astrophysical community to search for related species in the ISM. Very recently, diverse COMs, including HCOOH, $CH_3COOH$, and a variety of amino acids, have been detected through mass spectrometry in the samples of the near-Earth carbonaceous (C-type) asteroid 162173 Ryugu, gathered and transported to Earth by the Hayabusa2 spacecraft (Naraoka et al. 2023).

The presence of prebiotic COMs within extraterrestrial material thus firmly suggests the existence of carboxylic acids of increasing complexity in the ISM, including amino acid–related species. Within this context, considerable efforts have been devoted to hunting for other acids, such as propenoic or acrylic acid ($CH_2CHCOOH$; Alonso et al. 2015), propanoic acid ($CH_3CH_2COOH$; Ilyushin et al. 2021), cyanoacetic acid ($CH_2CNCOOH$; Sanz-Novo et al. 2021), glycolic acid ($CH_2OHCOOH$; Blom & Bauder 1981; Jiménez-Serra et al. 2020), hydantoic acid ($C(O)OHCH_2NHC(O)NH_2$; Kolesniková et al. 2019), and glycine ($CH_2(NH_2)C(O)OH$; Combes et al. 1996; Hollis et al. 2003; Kuan et al. 2003; Cunningham et al. 2007; Jones et al. 2007; Jiménez-Serra et al. 2016, 2020), whose identification in the ISM remains elusive (Snyder et al. 2005).

In this work, we present the discovery in the ISM of carbonic acid, which has been detected toward the chemically rich G+0.693–0.027 (hereafter G+0.693) molecular cloud, located in the Galactic center. We performed the search for the two most stable conformers of the molecule, previously characterized in the laboratory by Mori et al. (2009, 2011), and we report the conclusive detection of the higher-energy *cis-trans* form and derive an upper limit to the column density for the *cis-cis* conformer. Additionally, we discuss their relative ratio, including a comparison with the well-known interstellar carboxylic acids, formic acid and acetic acid, toward several astronomical environments.

## 2. Observations

We searched for the *cis-cis* and *cis-trans* conformers of HOCOOH toward the Galactic center molecular cloud G+0.693. This prominent astronomical source is one of the main repositories of COMs in the Milky Way. To date, the analysis of the unbiased spectral survey conducted toward G+0.693 has resulted in the first interstellar detections of more than a dozen COMs (see, e.g., Rivilla et al. 2019, 2020, 2021a; Rodríguez-Almeida et al. 2021a; Rodríguez-Almeida et al. 2021b; Rivilla et al. 2021b; Zeng et al. 2021; Rivilla et al. 2022a, 2022b; Jimenez-Serra et al. 2022; Zeng et al. 2023).

This spectral survey was performed with the Yebes 40 m (Guadalajara, Spain) and IRAM 30 m (Granada, Spain) telescopes, and its sensitivity has recently been enhanced compared to previous works (e.g., Rivilla et al. 2021a; Rodríguez-Almeida et al. 2021a; Jimenez-Serra et al. 2022). For the observations, we employed the position-switching mode, centered at $\alpha = 17^h47^m22^s$, $\delta = -28°21'27''$, with the off position shifted by $\Delta\alpha = -885''$ and $\Delta\delta = 290''$.

The new Yebes 40 m observations (project 21A014; PI: Rivilla) comprised different observing runs performed between 2021 March and 2022 March. We employed the ultra-broadband Nanocosmos *Q*-band (7 mm) HEMT receiver that allows broadband observations (18.5 GHz) in two linear polarizations (Tercero et al. 2021). The backends are 16 fast Fourier transform spectrometers that provide a raw channel width of 38 kHz. Two distinct spectral setups were used, centered at 41.4 and 42.3 GHz and covering the whole *Q*-band (frequency range: 31.07−50.42 GHz). We initially examined and reduced the data by employing a Python-based script (Megías et al. 2023)[10] that uses the CLASS module within the GILDAS package. Hence, a systematic approach was followed for each observing day. We automatically fitted baselines using an iterative method that first masks the more visible lines using *sigma-clips* and then applies rolling medians and averages, interpolating the masked regions with splines. Afterward, the spectra were combined, averaged, and subsequently imported to MADCUBA (Martín et al. 2019). Note that we compared the spectra obtained using the different frequency setups to inspect possible line contamination from spurious lines and other technical artifacts. We finally smoothed the resulting spectra to 256 kHz, which translates into velocity resolutions of 1.5−2.5 km $s^{-1}$ in the range observed. We checked the flux density consistency between the new data and the previous Yebes 40 m survey (e.g., Zeng et al. 2020), obtaining a good match (within a 5% level). We have achieved an extremely high level of sensitivity, with rms noise levels lying between 0.25 and 0.9 mK across the whole *Q*-band at this spectral resolution in antenna temperature ($T_A^*$) scale, as the molecular emission toward G+0.693 is extended over the beam (Requena-Torres et al. 2006, 2008; Zeng et al. 2018, 2020). The half-power beamwidth (HPBW) of the telescope varies between ∼35″ and 55″ across the frequency range covered (Tercero et al. 2021).

The new IRAM 30 m observations (project 123-22; PI: Jiménez-Serra) were performed between 2023 February 1 and 18. We used several frequency setups to cover different spectral ranges of the E0 (3 mm) and E1 (2 mm) bands of the multiband millimeter-wave receiver Eight MIxer Receiver (EMIR). An initial spectral resolution of 195 kHz was achieved by using the fast Fourier transform spectrometer (FTS200). Each setup was slightly shifted in frequency in order to spot possible contamination of spurious lines from the image band. We covered three frequency ranges, 83.2−115.41, 132.28−140.39, and 142−173.81 GHz, and the HPBW is ∼14″–29″. We imported the spectra from CLASS to MADCUBA and subsequently compared the line intensities of the new astronomical data with those of previous observations (e.g., Rodríguez-Almeida et al. 2021a), obtaining an excellent consistency (within a 5% level). Afterward, we averaged the above data within MADCUBA by weighting the spectra according to their rms noise level. We then smoothed the resulting spectra to 615 kHz, which corresponds to velocity resolutions of 1.0−2.2 km $s^{-1}$ in the observed frequency range. All in all, we reached noise levels between 0.5 and 2.5 mK at 3 mm and 1.0 and 1.6 mK at 2 mm. For the frequency ranges that are not covered by the new observations, we kept our previous IRAM 30 m survey (further details are reported elsewhere; e.g., Rodríguez-Almeida et al. 2021a; Rivilla et al. 2022b).

## 3. Analysis and Results

### 3.1. Rotational Spectroscopy of Carbonic Acid

The spectroscopic data of HOCOOH were obtained from previous Fourier transform microwave and double resonance measurements carried out by Mori et al. (2009, 2011). The conformational landscape of this carboxylic acid shows three distinct conformational isomers or conformers, *cis-cis* (global

[10] https://github.com/andresmegias/gildas-class-python/

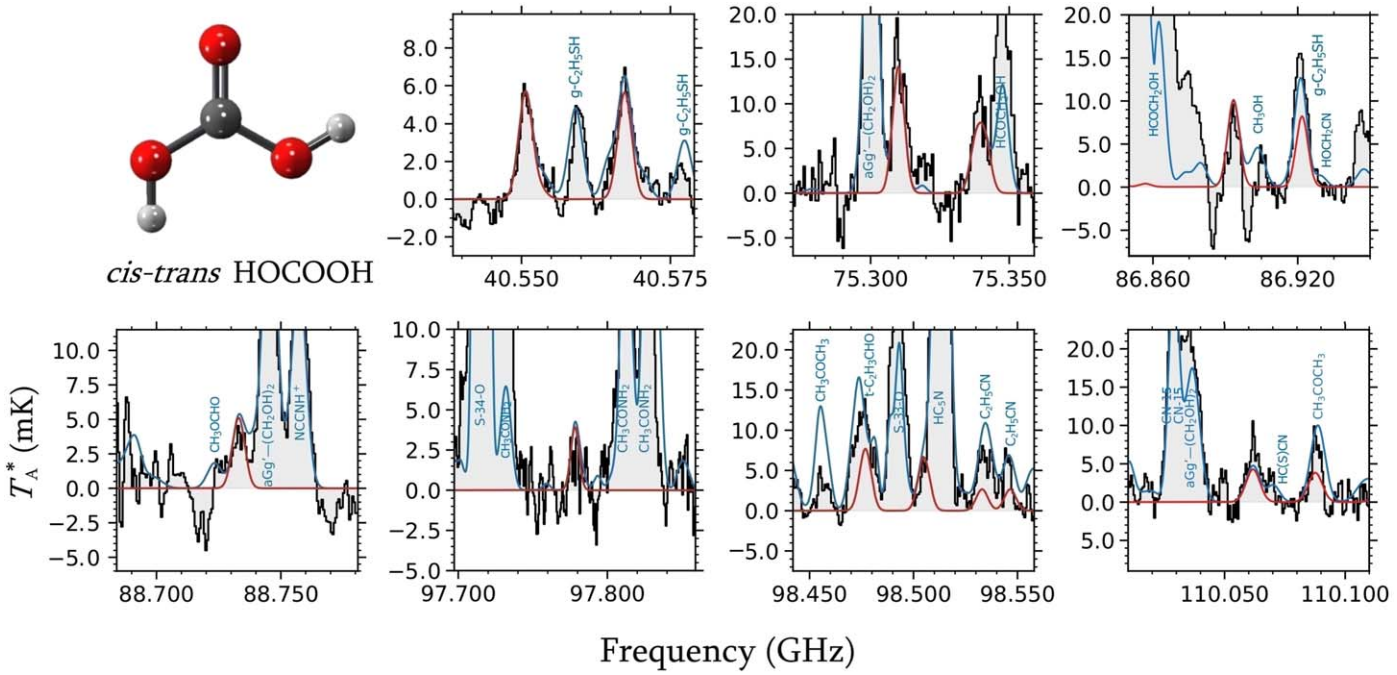


**Figure 1.** Selected transitions of *cis-trans* HOCOOH identified toward the G+0.693 molecular cloud (listed in Table 1). The result of the best LTE fit is shown with a red solid line, while the blue line shows the expected molecular emission from all of the molecular species identified to date in our survey. The observed spectra are plotted as gray histograms. The structure of *cis-trans* HOCOOH is also depicted (carbon atoms in gray, oxygen atoms in red, and hydrogen atoms in white).

minimum in energy), *cis-trans*, and *trans-trans* (located at 1.74 and 10.9 kcal mol$^{-1}$ higher in energy, respectively), although only the *cis-cis* and *cis-trans* forms have been measured in the laboratory. These two HOCOOH conformers are asymmetric tops close to the oblate limit (see Figures 1 and 2). Thus, according to the dipole moment selection rules, *a*- and *b*-type lines are permitted for the *cis-trans* conformer ($\mu_a = 1.0$ and $\mu_b = 2.9$ D, computed at the CCSD(T)/cc-pVQZ level; Mori et al. 2009), while only the *b*-type spectrum is observable for the *cis-cis* form. However, the latter exhibits an extremely low dipole moment ($\mu_b = 0.2$ D at the CCSD(T)/cc-pVQZ level; Mori et al. 2011), which hampered its detection in the first spectroscopic characterization of the isolated molecule (Mori et al. 2009). Consequently, we can foresee that only the direct identification of the *cis-trans* conformer will be feasible in the ISM, since its *b*-type dipole moment component is almost 15 times larger than that of *cis-cis* HOCOOH.

So far, only seven *b*-type *R*- and *Q*-branch transitions have been reported in the literature for *cis-cis* HOCOOH in the 6.1–41 GHz frequency range (Mori et al. 2009), while a total of 25 transitions, including different *a*- and *b*-type lines, have been measured for the *cis-trans* conformer from 4.8 to 65 GHz (Mori et al. 2011). We employed all of the available transition frequencies to perform a least-squares fit to a semirigid rotor Hamiltonian for each conformer separately (Watson's *A*-reduced Hamiltonian in $I^r$ representation). The resulting spectroscopic constants are listed in Table A1. We then extrapolated these results to higher frequencies (up to ∼120 GHz) in order to prepare separate line catalogs to search for both conformers in the ultrasensitive unbiased spectral survey toward G+0.693.

After performing the search, several lines of *cis-trans* HOCOOH were straightforwardly identified in the astronomical data (i.e., the detected transitions at ∼40 GHz were perfectly fitted by the predictions based exclusively on Mori et al. 2009; see Section 3.2 for more detailed information).

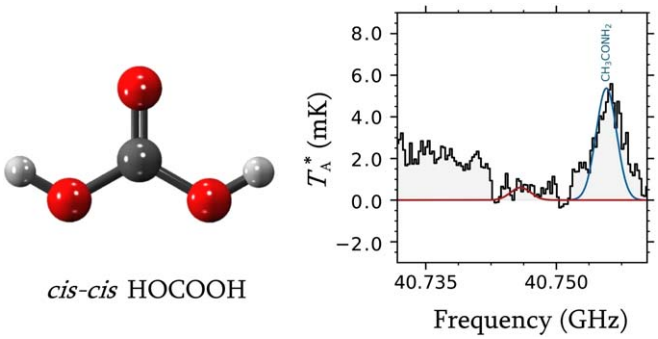


**Figure 2.** The LTE simulation of the *cis-cis* HOCOOH emission at the 3$\sigma$ upper limit column density derived toward G+0.693 using the physical parameters shown in Table 2 (in red) together with the expected molecular emission from all of the molecular species identified to date in our survey (in blue), both overlaid on the observations (black line and gray histogram). The features depicted correspond to the $3_{1,3}$–$2_{0,2}$ rotational transition. The structure of *cis-cis* HOCOOH is also shown.

Nevertheless, it is worth noticing that systematic discrepancies up to ∼5 km s$^{-1}$ were initially found for the higher-frequency astronomical lines (e.g., those at ∼110 GHz) when compared to our predictions. As expected, this fact points to the need for higher-order centrifugal distortion constants to perfectly reproduce the astronomical spectra, especially at frequencies higher than ∼90 GHz, since the available laboratory data are limited to 65 GHz. At this point, we employed pairs of *a*- and *b*-type transitions with $K_a = 0$, 1 ($J = 5$, 6, and 8) and $K_a = 1$, 2 ($J = 7$) that are merged into quadruply degenerated lines (four astronomical lines with excellent signal-to-noise ratio, S/N > 10) to perform a global fit together with the previous laboratory measurements (Mori et al. 2009, 2011). We treated the astronomical data using Pickett's SPFIT/SPCAT program suite (Pickett 1991) and fitted each observational line to a Gaussian profile to obtain its rest frequency. The weight of the

**Table 1**
Spectroscopic Information of the Selected Unblended or Slightly Blended Transitions of *cis-trans* HOCOOH Detected toward G+0.693 (Shown in Figure 1)

| Frequency (GHz) | Transition[a] | log $I$ ($nm^2$ MHz) | $g_u$ | $E_{LO}$ ($cm^{-1}$) | $E_{up}$ (K) | rms (mK) | $\int T_A^* dv$ (mK km $s^{-1}$) | S/N[b] | Comments[c] |
|---|---|---|---|---|---|---|---|---|---|
| 40.5511839 | $3_{1,3}$– $2_{1,2}$ | −6.0615 | 7 | 1.6 | 4.1 | 0.5 | 128.6 | 47.9 | Unblended |
| 40.5670170 | $3_{0,3}$–$2_{0,2}$ | −6.0615 | 7 | 1.6 | 4.1 | 0.5[d] | 164.6 | 61.3 | Slightly blended: $(CH_2OH)_2$ |
| 40.5674840 | $3_{1,3}$–$2_{0,2}$ | −5.1434 | 7 | 1.6 | 4.1 | | | | Slightly blended: $(CH_2OH)_2$ |
| 75.3102432 | $6_{1,6}$–$5_{1,5}$* | −5.1953 | 13 | 6.8 | 13.3 | 2.4 | 391.4 | 29.7 | Unblended◇ |
| 75.3102432 | $6_{0,6}$–$5_{1,5}$* | −4.2732 | 13 | 6.8 | 13.3 | | | | Unblended◇ |
| 75.3102432 | $6_{1,6}$–$5_{0,5}$* | −4.2732 | 13 | 6.8 | 13.3 | | | | Unblended◇ |
| 75.3102432 | $6_{0,6}$–$5_{0,5}$* | −5.1953 | 13 | 6.8 | 13.3 | | | | Unblended◇ |
| 75.3381091 | $5_{1,4}$–$4_{2,3}$* | −4.4608 | 11 | 6.0 | 9.7 | 2.4 | 228.4 | 17.3 | Unblended◇ |
| 75.3382086 | $5_{2,4}$–$4_{2,3}$* | −5.3723 | 11 | 6.0 | 9.7 | | | | Unblended◇ |
| 75.3413737 | $5_{1,4}$–$4_{1,3}$* | −5.3722 | 11 | 6.0 | 9.7 | | | | Unblended◇ |
| 75.3414732 | $5_{2,4}$–$4_{1,3}$* | −4.4607 | 11 | 6.0 | 9.7 | | | | Unblended◇ |
| 86.8938108 | $7_{0,7}$–$6_{0,6}$* | −5.0043 | 15 | 6.0 | 17.4 | 1.2 | 68.5 | 10.3 | Unblended◇ |
| 86.8938108 | $7_{0,7}$–$6_{1,6}$* | −4.0817 | 15 | 6.0 | 17.4 | | | | Unblended◇ |
| 86.8938108 | $7_{1,7}$–$6_{0,6}$* | −4.0817 | 15 | 6.0 | 17.4 | | | | Unblended◇ |
| 86.8938108 | $7_{1,7}$–$6_{1,6}$* | −5.0043 | 15 | 6.0 | 17.4 | | | | Unblended◇ |
| 86.9222625 | $6_{1,5}$–$5_{2,4}$* | −4.2356 | 13 | 8.5 | 16.3 | 1.2 | 343.2 | 51.7 | Blended: $HOCH_2CN$ and $g$-$C_2H_5SH$ |
| 86.9222651 | $6_{2,5}$–$5_{2,4}$* | −5.1504 | 13 | 8.5 | 16.3 | | | | Blended: $HOCH_2CN$ and $g$-$C_2H_5SH$ |
| 86.9223620 | $6_{1,5}$–$5_{1,4}$* | −5.1504 | 13 | 8.5 | 16.3 | | | | Blended: $HOCH_2CN$ and $g$-$C_2H_5SH$ |
| 86.9223647 | $6_{2,5}$–$5_{1,4}$* | −4.2356 | 13 | 8.5 | 16.3 | | | | Blended: $HOCH_2CN$ and $g$-$C_2H_5SH$ |
| 88.7332608 | $4_{4,1}$–$3_{3,0}$* | −4.4485 | 9 | 4.7 | 10.9 | 1.6 | 86.1 | 9.7 | Unblended |
| 97.7784440 | $4_{4,0}$–$3_{3,1}$* | −4.5160 | 9 | 4.5 | 11.1 | 1.4 | 50.1 | 6.5 | Unblended |
| 98.4770930 | $8_{0,8}$–$7_{0,7}$* | −4.8401 | 17 | 12.2 | 22.1 | 1.4 | 94.7 | 12.2 | Blended: $t$-$C_2H_3CHO$ |
| 98.4770930 | $8_{0,8}$–$7_{1,7}$* | −3.9172 | 17 | 12.2 | 22.1 | | | | Blended: $t$-$C_2H_3CHO$ |
| 98.4770930 | $8_{1,8}$–$7_{0,7}$* | −3.9172 | 17 | 12.2 | 22.1 | | | | Blended: $t$-$C_2H_3CHO$ |
| 98.4770930 | $8_{1,8}$–$7_{1,7}$* | −4.8401 | 17 | 12.2 | 22.1 | | | | Blended: $t$-$C_2H_3CHO$ |
| 98.5331999 | $6_{2,4}$–$5_{3,3}$* | −4.2241 | 13 | 9.9 | 18.8 | 1.4 | 174.2 | 22.5 | Blended: $C_2H_5CN$ |
| 98.5336969 | $6_{3,4}$–$5_{3,3}$* | −5.1255 | 13 | 9.9 | 18.8 | | | | Blended: $C_2H_5CN$ |
| 98.5462274 | $6_{2,4}$–$5_{2,3}$* | −5.1254 | 13 | 9.9 | 18.8 | 1.4 | 72.5 | 9.4 | Blended: $C_2H_5CN$ |
| 98.5467244 | $6_{3,4}$–$5_{2,3}$* | −4.2239 | 13 | 9.9 | 18.8 | | | | Blended: $C_2H_5CN$ |
| 110.0599685 | $9_{0,9}$–$8_{0,8}$* | −4.6965 | 19 | 15.5 | 27.3 | 1.8 | 107.4 | 10.8 | Unblended◇ |
| 110.0599685 | $9_{0,9}$–$8_{1,8}$* | −3.7733 | 19 | 15.5 | 27.3 | | | | Unblended◇ |
| 110.0599685 | $9_{1,9}$–$8_{0,8}$* | −3.7733 | 19 | 15.5 | 27.3 | | | | Unblended◇ |
| 110.0599685 | $9_{1,9}$–$8_{1,8}$* | −4.6965 | 19 | 15.5 | 27.3 | | | | Unblended◇ |
| 110.0880500 | $8_{1,7}$–$7_{2,6}$* | −3.8864 | 17 | 14.7 | 26.2 | 1.8 | 98.6 | 9.9 | Blended: $CH_3OCH_3$ |
| 110.0880500 | $8_{2,7}$–$7_{2,6}$* | −4.8046 | 17 | 14.7 | 26.2 | | | | Blended: $CH_3OCH_3$ |
| 110.0880500 | $8_{1,7}$–$7_{1,6}$* | −4.8046 | 17 | 14.7 | 26.2 | | | | Blended: $CH_3OCH_3$ |
| 110.0880500 | $8_{2,7}$–$7_{1,6}$* | −3.8864 | 17 | 14.7 | 26.2 | | | | Blended: $CH_3OCH_3$ |

**Notes.**
[a] The rotational energy levels are labeled using the conventional notation for asymmetric tops, $J_{K_a,K_c}$, where $J$ denotes the angular momentum quantum number, and $K_a$ and $K_c$ are projections of $J$ along the $a$ and $c$ principal axes. Lines that have been measured for the first time in the present astronomical data set are marked with an asterisk.
[b] The S/N is calculated from the integrated signal ($\int T_A^* dv$) and noise level $\sigma = \text{rms} \times \sqrt{\delta v \times \text{FWHM}}$, where $\delta v$ is the velocity resolution of the spectra, and the FWHM is fitted from the data.
[c] We denote as "unblended" lines that are not contaminated by other species and use a diamond symbol for those that are (auto)blended with another transition of *cis-trans* HOCOOH.
[d] For those transitions that are partially or fully coalesced, we provide the integrated intensity and S/N of the mean observed line rather than the value of each rotational transition, which is given only once for each group of transitions. The spectroscopic information was obtained from ctHOCOOH.cat, which is provided as Supporting Information.

purely astronomical lines was fixed to a much higher value than that used for the laboratory data; we employed 0.3 MHz, which corresponds to ∼1 km $s^{-1}$ at 100 GHz. The derived spectroscopic parameters for the global fit of *cis-trans* HOCOOH are listed in the third column of Table A1. The sextic centrifugal distortion constant $\Phi_J$ was determined from the fit, which enabled us to improve the predictions for the higher $J$ transitions. Finally, we prepared a new catalog for the *cis-trans* conformer (ctHOCOOH.cat, provided as Supporting Information in the common JPL SPFIT/SPCAT format; an example table, Table A3, is also given in Appendix A1), which was used in the following subsection to confirm the detection and derive the physical parameters of the molecule. This catalog can also be directly employed to search for *cis-trans* HOCOOH toward other astronomical sources.

### 3.2. Detection of cis-trans Carbonic Acid and Search for the cis-cis Conformer

Once we imported the spectroscopic catalog of HOCOOH into the MADCUBA package (Martín et al. 2019), the identification of the astronomical lines was carried out using the Spectral Line Identification and Modeling (SLIM) tool, which works under the assumption of local thermodynamic equilibrium (LTE) excitation to generate the synthetic spectra.

**Table 2**
Derived Physical Parameters for HCOOH, $CH_3COOH$, and HOCOOH toward the G+0.693 Molecular Cloud

| Molecule | Formula | $N$ ($\times 10^{14}$ cm$^{-2}$) | $T_{ex}$ (K) | $v_{LSR}$ (km s$^{-1}$) | FWHM (km s$^{-1}$) | Abundance[a] ($\times 10^{-10}$) | Ref.[b] |
|---|---|---|---|---|---|---|---|
| *Trans* formic acid | *t*-HCOOH | $2.0 \pm 0.4$ | $10 \pm 1$ | $68 \pm 2$ | $22 \pm 5$ | $15 \pm 4$ | (1) |
| *Cis* formic acid[c] | *c*-HCOOH | $0.017 \pm 0.002$ | 10[d] | 69[d] | $17 \pm 3$ | $0.13 \pm 0.02$ | (2) |
| Acetic acid | $CH_3COOH$ | $0.42 \pm 0.02$ | $17 \pm 2$ | $69.5 \pm 0.5$ | 21[d] | $3.1 \pm 0.2$ | (2) |
| *Cis-trans* carbonic acid | *ct*-HOCOOH | $0.064 \pm 0.004$ | $7.2 \pm 0.6$ | $69.8 \pm 0.8$ | 20[d] | $0.47 \pm 0.03$ | (2) |
| *Cis-cis* carbonic acid | *cc*-HOCOOH | $\leqslant 1.6$ | 7.2 | 69.8 | 20 | $\leqslant 12$ | (2) |

**Notes.**
[a] We adopted $N_{H_2} = 1.35 \times 10^{23}$ cm$^{-2}$ from Martín et al. (2008).
[b] References: (1) Rodríguez-Almeida et al. (2021a); (2) this work.
[c] For *c*-HCOOH, we present a tentative detection.
[d] Value fixed in the fit.

In Table 1, we collect the most intense—according to the integrated S/N—unblended or slightly blended transitions of *cis-trans* HOCOOH detected toward G+0.693. The rest of the lines, which appear blended with brighter transitions from other species, show predicted intensities that are consistent with the observed spectra considering the contribution from all of the species previously identified toward G+0.693. In Figure 1, we depict the fitted line profiles of *cis-trans* HOCOOH (red solid line) with integrated S/N > 6. Among them, we managed to detect up to four pairs of lines of *cis-trans* HOCOOH, corresponding to different $K_a = 0$, 1, and 2 progressions, which almost perfectly reproduce the observations. Two of them are completely clean, and their relative line intensities are well fitted (first and second panels of Figure 1). For the other two pairs (third and seventh panels), one line appears unblended, and the other reproduces the observed spectra once the contribution from all other identified species is considered (blue solid line).

Then, we used all of the above lines to carry out the corresponding LTE fit and obtain the physical parameters of the emission of *cis-trans* HOCOOH. We employed the AUTOFIT tool within MADCUBA-SLIM (Martín et al. 2019), which performs a nonlinear least-squares fit of the simulated LTE spectra to the observed data. Note that we also considered the predicted emission from the already-identified molecules in the same frequency region. The best-fitting LTE model for *cis-trans* HOCOOH gives a molecular column density of $N = (6.4 \pm 0.4) \times 10^{12}$ cm$^{-2}$, an excitation temperature of $T_{ex} = 7.2 \pm 0.6$ K, a radial velocity of $v_{LSR} = 69.8 \pm 0.8$ km s$^{-1}$, and an FWHM of 20 km s$^{-1}$ (fixed in the fit, according to the line width of the low-frequency *Q*-band lines). This value of the molecular column density is transcribed into a molecular abundance with respect to molecular hydrogen of $\sim 4.7 \times 10^{-11}$, adopting $N(H_2) = 1.35 \times 10^{23}$ cm$^{-2}$ from Martín et al. (2008).

We have also carried out a complementary population or rotational diagram analysis (Goldsmith & Langer 1999), as implemented in MADCUBA, using the velocity-integrated intensity over the line width (Rivilla et al. 2021a). Following this approach, we derived physical parameters for *cis-trans* HOCOOH that are in perfect agreement with the AUTOFIT analysis: $N = (6.5 \pm 1.1) \times 10^{12}$ cm$^{-2}$ and $T_{ex} = 7.5 \pm 0.5$ K. The results are shown in Figure 3.

Afterward, we searched for the global minimum in energy *cis-cis* HOCOOH, but it was not detected in the current line survey due to its low dipole moment. To derive an upper limit to the column density, we adopted parameters obtained for the *cis-trans* conformer (see Table 2), leaving the column density as the only free parameter. Then, we used the brightest transition according to the simulated LTE spectrum that is not contaminated by other species. The brightest transition appears contaminated with the emission of $C_2H_3CN$ and $CH_3CHO$. Thus, the chosen rotational transition for *cis-cis* HOCOOH is $3_{1,3}$–$2_{0,2}$ (located at 40.7460 GHz), from which we obtained a $3\sigma$ upper limit to the column density of $N \leqslant 1.6 \times 10^{14}$ cm$^{-2}$ that does not produce any overly bright features at other frequencies. In terms of the molecular abundance with respect to $H_2$, the above value is translated into an upper limit of $\leqslant 1.2 \times 10^{-9}$, which further constrains the abundance of *cis-cis* HOCOOH in the ISM. The results of the LTE fits are listed in Table 2.

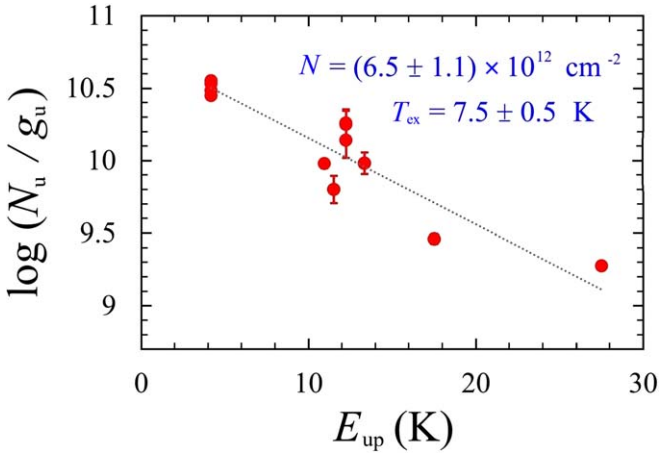


**Figure 3.** Rotational diagram of *cis-trans* HOCOOH using the unblended transitions (depicted by red dots) reported in Table 1. The gray dotted line corresponds to the best linear fit to the data points. The derived values for the molecular column density, $N$, and the excitation temperature, $T_{ex}$, are shown in blue.

### 3.3. Detection of $CH_3COOH$ and Tentative Detection of *c*-HCOOH

Acetic acid, $CH_3COOH$, was previously searched for toward G+0.693 (an upper limit to the column density was reported in Requena-Torres et al. 2006). Here we perform an accompanying search using the current astronomical data set, and $CH_3COOH$ is now unequivocally detected (see Figure 4). We present the complete LTE analysis in Appendix B (see Table B1), and the derived physical parameters are collected in

Table 2 along with the physical parameters of HCOOH and HOCOOH.

Regarding formic acid, HCOOH, the *trans* conformer is commonly found in regions with some degree of chemical complexity, including G+0.693 (Rodríguez-Almeida et al. 2021a; García de la Concepción et al. 2022). However, the less stable *cis* conformer has only been found toward sources displaying specific physical and chemical properties, such as the Orion Bar photodissociation region (Cuadrado et al. 2016) and the cold molecular clouds L483 (Agúndez et al. 2019) and B5 (Taquet et al. 2017). In this work, we managed to tentatively detect *cis*-HCOOH using the new ultradeep observations of G+0.693. We present the corresponding LTE analysis in Appendix C (see Table C1 and Figure 5), and we list the derived physical parameters in the second row of Table 2.

## 4. Discussion

### 4.1. Conformational Isomerism of HOCOOH

On the basis of the derived molecular abundances (see Table 2), we obtain a *cis-cis*/*cis-trans* HOCOOH abundance ratio of $\leqslant$25, which is relatively lower than the *trans/cis* upper limit ratio obtained for the related HCOOH in G+0.693 ($\sim$117) considering the tentative detection in G+0.693 presented here and in the high-mass star-forming region G31.41+0.31 ($\geqslant$90; García de la Concepción et al. 2022). Nevertheless, this fact can be easily rationalized in terms of the different relative electronic energies between the two low-lying conformers of HCOOH ($\Delta E(cis/trans) = 4.04$ kcal mol$^{-1}$; García de la Concepción et al. 2022) and HOCOOH ($\Delta E$(*cis-trans*/*cis-cis*) = 1.71 kcal mol$^{-1}$; Mori et al. 2009). A similar but more pronounced behavior was observed between HCOOH and HC(O)SH, since the relative electronic energy between the two conformers of the S-bearing acid is only 0.68 kcal mol$^{-1}$, which is translated in a much lower *trans/cis* abundance ratio of $\sim$3.7 (García de la Concepción et al. 2022).

Similarly to HCOOH, HOCOOH can also exhibit *trans/cis* rotational or conformational isomerism (Pettersson et al. 2002; Maçôas et al. 2005; Tsuge & Khriachtchev 2015; García de la Concepción et al. 2022), and the stability of each conformer is driven by the formation of stabilizing intramolecular hydrogen bonds. These types of isomerization processes have already been proven to be feasible under ISM conditions thanks to multidimensional ground-state quantum tunneling effects (García de la Concepción et al. 2022). Therefore, given that HOCOOH can also undergo quantum tunneling (Wagner et al. 2016), we suggest that the *cis-cis*/*cis-trans* ratio observed in the ISM may be explained in terms of the relative stability of the conformers, which is consistent with the low abundance reported for the high-energy *cis-trans* HOCOOH. For several stereoisomers detected toward G+0.693, we have observed that the derived relative isomeric ratio match that predicted under thermodynamic equilibrium conditions, further supporting the above statement, highlighting *Z* and *E* isomers of cyanomethanimine (HNCHCN), whose relative ratio was rationalized theoretically under ISM conditions also based on quantum tunneling effects (García de la Concepción et al. 2021), and the *Ga* and *Aa* conformers of *n*-propanol (*n*-$C_3H_7OH$; Jimenez-Serra et al. 2022).

Furthermore, although we have shown that the detection of *cis-cis* HOCOOH by means of its rotational spectra is, at the very least, a challenging task, we can now shed light on the total abundance of the molecule based on the detection of the higher-energy *cis-trans* form, which exhibits a sizable dipole moment. This fact shall guide the astronomical community to perform future searches for referable systems toward sources exhibiting high kinetic temperatures ($T_{kin}$), such as Galactic center molecular clouds (i.e., G+0.693), hot cores, and corinos, which can populate higher-energy species efficiently if the energy difference is not exorbitant and assuming a thermodynamic population.

### 4.2. Relative Abundance of Carboxylic Acids in Space

To put HOCOOH in a broader astrochemical context, we can compare its abundance in G+0.693 with the abundance of the only two detected carboxylic acids in the ISM so far, also detected toward G+0.693: HCOOH and $CH_3COOH$.

As shown in Table 2, we obtained a $CH_3COOH$/*ct*-HOCOOH ratio of $\sim$7, showing that $CH_3COOH$ is not significantly more abundant than the high-energy form of HOCOOH toward G+0.693. Moreover, we found that *cis-trans* HOCOOH is $\sim$31 times less abundant than *t*-HCOOH and, at the same time, $\sim$four times more abundant than *c*-HCOOH toward this astronomical source. Nevertheless, if we consider the upper limit derived for the *cis-cis* form of HOCOOH and the aforementioned conformational isomerism, its abundance is expected to be of the same order as that of *t*-HCOOH. Thus, carbonic acid possibly emerges as a ubiquitous and abundant O-bearing COM in the ISM, although it has gone unnoticed so far.

At this point, the detection of both HCOOH and $CH_3COOH$ toward G+0.693 allows us to provide a rough comparison with the concentration of these acids in the envelope of the neighbor star-forming region Sgr B2(N) (Belloche et al. 2013), as well as in asteroids (in the Ryugu material; Naraoka et al. 2023) and comets (67P/C-G; Altwegg et al. 2016; Drozdovskaya 2019). The results are summarized in Table 3 and Figure 6 (Appendix D). As can be seen, the HCOOH/$CH_3COOH$ ratio derived in the Ryugu material ($\sim$1.7; Naraoka et al. 2023) is consistent with the one obtained through radio astronomical observations in both G+0.693 ($\sim$4.4) and the envelope of Sgr B2(N) ($\sim$1.4) within an factor of 3. In comparison, a larger amount of HCOOH is available in the G+0.693 molecular cloud, which will most likely react to form more complex derivatives at later stages. For $CH_3COOH$, the mass spectrometric measurements carried out with the ROSINA instrument (Drozdovskaya 2019) were not able to differentiate between acetic acid and its isomers, methyl formate ($HCOOCH_3$), glycolaldehyde ($CH_2OHCHO$), and ethenediol $(CHOH)_2$. Thus, we need to include these isomers ($C_2O_2H_4$) to properly analyze the abundance of $CH_3COOH$ in the volatile cometary material of 67P/C-G, which exhibits a similar HCOOH/$C_2O_2H_4$ ratio ($\sim$0.4) compared with that obtained in G+0.693 ($\sim$0.24). Meanwhile, in Sgr B2(N), a ratio 1 order of magnitude lower is observed due to the large abundance of methyl formate toward this source. Therefore, our results suggest a relationship between the relative molecular abundance of carboxylic acids in the ISM and that found in minor bodies of the solar system, suggesting that they survive the star formation process (Rivilla et al. 2021a).

The fact that the identification of HOCOOH in extraterrestrial bodies (e.g., asteroids and comets) remains elusive is not surprising. In this context, the debate about whether HOCOOH

could persist long enough to enable its spectroscopic characterization remained open for many years, since this elusive molecule rapidly decomposes into $CO_2$ and $H_2O$ (Ghoshal & Hazra 2015) or upon deprotonation in solution. This significantly affects its tractability in aqueous solution—the presence of just two catalytically active water molecules leads to decomposition (Loerting et al. 2000)—as well as in the presence of other organic molecules (Ghoshal & Hazra 2015). In this context, aqueous alteration might have happened in the Ryugu samples, but it is not likely to have occurred to an important extent in comet 67P/C-G, whose composition is expected to be more pristine. However, gaseous HOCOOH presents a rather surprising kinetic stability in the absence of water (Loerting et al. 2000). Fortunately, it was identified at last in gas-phase isolation conditions by Mori et al. (2009, 2011), which guided us to achieve the present interstellar discovery. In addition, although to our knowledge HOCOOH has not been searched for in the volatile cometary material of 67P/C-G, its possible identification might have a problem with the contamination of its mass peak with ethylene glycol, $(CH_2OH)_2$ (Rubin et al. 2019), which shares the same molecular mass of HOCOOH (63.02 u). Thus, it could indeed be present in the extraterrestrial material of asteroids and comets, but it remains unidentified.

### 4.3. Interstellar Formation of HOCOOH

The formation of HOCOOH in the ISM has been the subject of a plethora of recent experimental and theoretical studies (e.g., Gerakines et al. 2000; Zheng & Kaiser 2007; Baltrusaitis & Grassian 2010; Oba et al. 2010; Ioppolo et al. 2021). Oba et al. (2010) investigated the formation of HOCOOH on dust-grain surfaces from the reaction between CO and the radical species OH to form both *cis* and *trans* HOCO at low temperatures (Lester et al. 2001; Noble et al. 2011; Nguyen et al. 2012; Ruaud et al. 2015; Tachikawa & Kawabata 2016; reactions 1, 2):

$$\mathrm{CO} + \mathrm{OH} \rightarrow \mathrm{trans} - \mathrm{HOCO}, \quad (1)$$

$$\mathrm{CO} + \mathrm{OH} \rightarrow \mathrm{cis} - \mathrm{HOCO}, \quad (2)$$

$$\mathrm{trans} - \mathrm{HOCO} + \mathrm{OH} \rightarrow \mathrm{HOCOOH}, \quad (3)$$

$$\mathrm{cis} - \mathrm{HOCO} + \mathrm{OH} \rightarrow \mathrm{HOCOOH}. \quad (4)$$

Once HOCO is formed, it may fall apart to yield $H + CO_2$ or further react with additional OH radicals yielding HOCOOH (reactions 3, 4). This surface pathway has already been suggested as one of the key plausible routes to the formation of HOCOOH in cold dense molecular clouds (Ioppolo et al. 2021). It again emphasizes the relevance of radical addition reactions, in particular those involving reactions between the OH radical and neutral species in interstellar surface chemistry (e.g., Molpeceres & Rivilla 2022). In addition, although the most stable form of the HOCO radical, *trans*-HOCO, remains undetected toward G+0.693, based on the derived integrated intensity $3\sigma$ upper limit to its column density of $N \leqslant 1.2 \times 10^{12}$ cm$^{-2}$ (using entry 45517 of the Cologne Database for Molecular Spectroscopy, CDMS, catalog; Müller et al. 2005), we obtain a *ct*-HOCOOH/*t*-HOCO abundance ratio of ~5.3. This ratio could be rationalized based on the low abundance expected for such intermediate and highly reactive species in the suggested formation pathways, which may be formed but will rapidly react to form more complex products.

Moreover, HOCOOH has been hinted at as the main reaction product of the energetic processing of $H_2O/CO_2$ icy mixtures (in different proportions), highlighting the electron-induced formation route proposed by Zheng & Kaiser (2007), which is initiated by Reactions (5) and (6), followed by the radical association with OH (see Reaction (4) above):

$$\mathrm{H_2O} + \mathrm{e^-} \rightarrow \mathrm{H} + \mathrm{OH} + \mathrm{e^-}, \quad (5)$$

$$\mathrm{H} + \mathrm{CO_2} \rightarrow \mathrm{cis} - \mathrm{HOCO}. \quad (6)$$

Alternatively, the production of HOCOOH may occur through atomic H abstraction from HCOOH (Markmeyer et al. 2019; Molpeceres et al. 2022), which is efficiently formed in the ISM (Qasim et al. 2019), followed by radical addition (i.e., HOCO + OH). Therefore, sources that are reservoirs of large amounts of HCOOH are excellent targets for confirming the detection of HOCOOH.

To our knowledge, apart from the direct $CO_2 + H_2O$ reaction that shows high activation barriers (Baltrusaitis & Grassian 2010), the gas-phase formation routes of HOCOOH remain unexplored. For instance, we can suggest ion–molecule reactions between positive ions, such as the detected $HOCO^+$ (Thaddeus et al. 1981; Majumdar et al. 2018), which is also present in G+0.693 (Armijos-Abendaño et al. 2015), or even $HCOOH^+$, and neutral molecules.

Hence, although HOCOOH is most likely formed via OH radical addition to HOCO on the surface of dust grains, further theoretical effort is needed to build complete chemical reaction networks to understand the presence of HOCOOH in space and decipher which of the above formation pathways prevail over the rest. Finally, HOCOOH represents the first molecule with more than two O atoms detected so far in the ISM. Thus, the current investigation expands our knowledge of O-bearing COMs and opens the window for the detection of other interstellar molecules containing multiple oxygen atoms.

## 5. Summary and Conclusions

Modern radio astronomical facilities and laboratory work are steadily pushing the limits of the chemical complexity found in the ISM. However, for certain families of molecules (i.e., carboxylic acids), the count of identified interstellar species has remained unchanged for more than two decades. In this context, *cis-trans* HOCOOH has been detected at last in the ISM toward the G+0.693 Galactic center molecular cloud and stands as the first interstellar molecule containing three O atoms. We derive a molecular column density for this conformer of $N = (6.4 \pm 0.4) \times 10^{12}$ cm$^{-2}$, which is translated into a molecular abundance with respect to molecular $H_2$ of $4.7 \times 10^{-11}$. Although the available laboratory measurements were limited to 65 GHz, we used our spectral line survey as a "conventional" laboratory spectrum and managed to directly detect several clear and unblended spectroscopic features in the radio astronomical data (between 75 and 120 GHz). This fact further allowed us to slightly improve the available set of rotational spectroscopic constants of *cis-trans* HOCOOH. We also report the nondetection of the more stable *cis-cis* HOCOOH, showing an upper limit to the molecular abundance with respect to $H_2$ of $\leqslant 1.2 \times 10^{-9}$ due to the huge impact that its low dipole moment has on the overall detectability of the conformer. Nevertheless, based on the derived upper limit, it is still likely that *cis-cis* HOCOOH is rather abundant. We suggest that it may be efficiently formed under interstellar

**Table 3**
Abundances and Ratio between Formic and Acetic Acid toward Different Astronomical Environments

| Source | $N$(*t*-HCOOH) ($cm^{-2}$) | $N(CH_3COOH)$ ($cm^{-2}$) | $N(C_2O_2H_4)$[c] ($cm^{-2}$) | $\frac{t-HCOOH}{CH_3COOH}$ | $\frac{t-HCOOH}{C_2O_2H_4}$ | Ref.[d] |
|---|---|---|---|---|---|---|
| G+0.693 | $(2.0 \pm 0.4) \times 10^{14}$ | $(4.5 \pm 0.2) \times 10^{13}$ | $(8.4 \pm 0.6) \times 10^{14}$ | 4.4 | 0.24 | (1) |
| Sgr B2(N) | $(1.5 \pm 0.2) \times 10^{16}$ | $(1.1 \pm 0.1) \times 10^{16}$ | $(4.5 \pm 0.5) \times 10^{17}$ | 1.4 | 0.03 | (2) |
| 67P/C-G | $0.013 \pm 0.008$[a] | – | $0.034 \pm 0.002$ | – | 0.4 | (3) |
| Ryugu (A0106) | $(9.47 \pm 10) \times 10^{3}$[a] | $(5.7 \pm 1.5) \times 10^{3}$ | – | 1.7 | – | (4) |

**Notes.**
[a] In 67P/C-G, the derived abundance is relative to $H_2O$ (percent).
[b] In the hot-water extract (A0106) of Ryugu, the abundance is reported in nmol $g^{-1}$.
[c] The relative abundance derived in 67P/C-G refers to all of the $C_2O_2H_4$ isomers, and, apart from $CH_3COOH$, it also includes the isomers methyl formate ($HCOOCH_3$), glycolaldehyde ($CH_2OHCHO$), and ethenediol $(CHOH)_2$ (only detected toward G+0.693).
[d] References: (1) Rodríguez-Almeida et al. (2021a), Rivilla et al. (2022a), and this work; (2) Belloche et al. (2013); (3) Drozdovskaya (2019); (4) Naraoka et al. (2023).

conditions, most likely via OH radical addition of HOCO on the surface of dust grains. Moreover, we obtained a *cis-cis*/*cis-trans* ratio of $\leqslant$25, in good agreement with the *trans*/*cis* ratio observed for the related HCOOH in G+0.693 based on the larger energetic difference between both HCOOH conformers. We found that *cis-trans* carbonic acid is ∼31 and 7 times less abundant than *t*-HCOOH and $CH_3COOH$, respectively, toward this astronomical source, but it is also ∼4 times more abundant than *c*-HCOOH. In addition, our comparison between the abundance of HCOOH and $CH_3COOH$ in different astronomical environments, including star-forming regions, asteroids, and comets, enabled us to establish an overall good correlation between the relative molecular abundance of carboxylic acids.

The interstellar discovery of carbonic acid (HOCOOH) presented in this work provides relevant insight into the actual degree of chemical complexity of the ISM and will have significant implications for unraveling the role of HOCOOH within interstellar carbon and oxygen chemistry based on the large amount of HOCOOH that might be lurking in space. This study will also pave the way to performing new harmonized observational, theoretical, and laboratory investigations targeting astronomical candidates that exhibit an extremely low dipole moment (e.g., *cis-cis* HOCOOH) based on the detection of other moderately higher-energy conformers with sizable dipole moments. Hence, we now open the door to achieving indirect interstellar identifications of conformers that remained undetectable to radioastronomy, especially toward high-$T_{kin}$ sources such as Galactic center molecular clouds (i.e., G+0.693) or hot cores and corinos, which are capable of populating these high-energy species efficiently.

## Acknowledgments

We are grateful to the IRAM 30 m and Yebes 40 m telescope staff for their help during the different observing runs. The 40 m radio telescope at Yebes Observatory is operated by the Spanish Geographic Institute (IGN; Ministerio de Transportes, Movilidad y Agenda Urbana). IRAM is supported by INSU/CNRS (France), MPG (Germany), and IGN (Spain). M.S.N. is thankful for funding from the European Union—NextGenerationEU, Ministerio de Universidades and the University of Valladolid under a postdoctoral Margarita Salas Grant, and also acknowledges funding from the Spanish Ministry of Science and Innovation (PID2020-117742GB-I00). V.M.R., I.J.-S., J.M.-P., L.C., A.M., and A.M.-H. acknowledge financial support from project Nos. RYC2020-029387-I and PID2019-105552RB-C41 funded by the Spanish Ministry of Science and Innovation/State Agency of Research MCIN/AEI/10.13039/501100011033. A.M. has received support from Spanish project No. MDM-2017-0737-19-2 and grant PRE2019-091471, funded by MCIN/AEI/10.13039/501100011033 and by "ESF Investing in your future." A.M.-H. acknowledges funds from grant MDM-2017-0737 Unidad de Excelencia "María de Maeztu" Centro de Astrobiología (CAB, INTA-CSIC). D.S.A. acknowledges the funds provided by the Consejo Superior de Investigaciones Científicas (CSIC) and the Centro de Astrobiología (CAB) through project 20225AT015 (Proyectos intramurales especiales del CSIC). P.d.V. and B.T. are thankful for the support from the Spanish Ministerio de Ciencia e Innovación (MICIU) through project PID2019-107115GB-C21. B.T. also thanks the Spanish MICIU for funding support from grant PID2019-106235GB-I00.

*Software:* (1) Madrid Data Cube Analysis (MADCUBA) on ImageJ is a software developed at the Center of Astrobiology (CAB) in Madrid, version 9.3.10 (04/05/2023), http://cab.inta-csic.es/madcuba/; Martín et al. (2019). (2) GILDAS package, https://www.iram.fr/IRAMFR/GILDAS. (3) Python, https://www.python.org. (4) Pickett's SPFIT/SPCAT program suite, https://spec.jpl.nasa.gov/; Pickett (1991).

## Appendix A
## Spectroscopic Details and Complementary Tables

In Table A1, we list the experimental constants for the ground state of *cis-cis* and *cis-trans* conformers of carbonic acid. In the third column, we report the results of the new global fit, including lines from the correctly weighted astronomical data, which have been measured for the first time in space.

Regarding the *cis-cis* conformer of HOCOOH ($C_{2v}$ symmetry), as reported in Mori et al. (2011), the rotational energy levels must be evaluated carefully, since this conformer has one pair of equivalent protons (obeying Fermi–Dirac statistics). Therefore, the existence of nuclear statistics is key in the determination of the relative intensities of rotational transitions; the levels will be divided into those where the rotational functions are symmetric with respect to a rotation around the *b*-symmetry axis ($K_a$, $K_c$ equals "even, even" or "odd, odd" para levels) and those with symmetric rotational functions ($K_a$, $K_c$ equals "even, odd" or "odd, even" ortho levels). Thus,

the proper nuclear statistical weight is 1:3, and at low temperatures, both ortho and para levels should be analyzed separately.

In Table A2, we provide the rotational ($Q_r$) partition function of the ground state of conformers *cis-cis* and *cis-trans*, which are mandatory to obtain reliable line intensities. We used SPCAT (Pickett 1991) to estimate the values of $Q_r$ from first principles at the conventional temperatures as implemented in the JPL database (Pickett et al. 1998) and an additional temperature of 5 K using the rotational spectroscopic parameters reported in Table A1 and Equation (3.67) of Gordy & Cook (1984). An example table (Table A3) for the generated ctHOCOOH.cat file is also provided.

**Table A1**
Experimental Spectroscopic Parameters for the Ground State of *cis-cis* (cc) and *cis-trans* (ct) HOCOOH (*A* Reduction, $I^r$ Representation)

| Parameter | *cis-cis* (cc)[f] | *cis-trans* (ct)[f] | Global Fit (ct)[h] |
|---|---|---|---|
| $A$[a] | 11,997.0646 (22) | 11,778.6808 (34) | 11,778.6801 (31) |
| $B$ | 11,308.3818 (14) | 11,423.1345 (32) | 11,423.1340 (30) |
| $C$ | 5813.82769 (71) | 5792.0741 (22) | 5792.0740 (21) |
| $\Delta_J$ | 6.371 (72) | 5.74 (18) | 5.64 (18) |
| $\Delta_{JK}$ | −2.13 (95) | −1.16 (79) | −1.14 (72) |
| $\Delta_K$ | 6.42 (79) | 8.14 (74) | 8.18 (68) |
| $\delta_J$ | 2.618[g] | 2.618 (83) | 2.616 (77) |
| $\delta_K$ | 6.28 | 6.28 (31) | 6.30 (28) |
| $\Phi_J$ | … | … | 5.3 (15) |
| $N$[b] | 7 | 25 | 41 |
| $\sigma$[c] | 1.0 | 8.6 | 25.8 |
| $\sigma_w$[d] | 0.98 | 0.86 | 0.81 |
| $\Delta E$[e] | 0.0 | 1.71 | 1.71 |

**Notes.** Standard errors in parentheses are displayed in units of the last digit.
[a] $A$, $B$, and $C$ represent the rotational constants (in MHz); $\Delta_J$, $\Delta_{JK}$, $\Delta_J$, $\delta_J$, and $\delta_K$ are the quartic centrifugal distortion constants (in kHz); and $\Phi_J$ is a sextic centrifugal distortion constant (in Hz).
[b] $N$ is the number of measured transitions.
[c] $\sigma$ is the rms deviation of the fit (kHz).
[d] $\sigma_w$ is the unitless (weighted) deviation of the fit. Their values are close to the $1\sigma$ standard uncertainties, since the unitless (weighted) deviation of the fit is very close to 1.0.
[e] $\Delta E$ is the energy calculated at the CCSD(T)/cc-pVQZ level (in kcal mol$^{-1}$; Mori et al. 2009).
[f] Spectroscopic parameters derived from the frequency measurements reported in Mori et al. (2009, 2011).
[g] Values fixed to that of *cis-trans* carbonic acid.
[h] Global fit of *cis-trans* carbonic acid, where newly measured astronomical lines are also included.

**Table A2**
Rotational Partition Function of *cis-cis* (cc) and *cis-trans* (ct) Carbonic Acid

| $T$ (K) | $Q_r$(cc) | log$Q_r$(cc) | $Q_r$(ct) | log$Q_r$(ct) |
|---|---|---|---|---|
| 5.000 | 68.3830 | 1.8349 | 68.7904 | 1.8375 |
| 9.375 | 174.039 | 2.2406 | 175.082 | 2.2432 |
| 18.75 | 489.828 | 2.6900 | 492.771 | 2.6926 |
| 37.50 | 1382.12 | 3.1405 | 1390.43 | 3.1432 |
| 75.00 | 3905.06 | 3.5916 | 3928.54 | 3.5942 |
| 150.0 | 11042.1 | 4.0431 | 11108.4 | 4.0457 |
| 225.0 | 20282.4 | 4.3071 | 20409.2 | 4.3098 |
| 300.0 | 31188.0 | 4.4940 | 31430.9 | 4.4974 |

**Note.** We used $J = 200$ as the maximum $J$ value.

**Table A3**
Example Table of the .cat File Provided for *cis-trans* HOCOOH (ctHOCOOH.cat) in the JPL SPFIT/SPCAT Format

| Frequency (MHz) | Error[a] (MHz) | log Int.[b] ($nm^2$ MHz) | DR[c] | $E_{LO}$[d] ($cm^{-1}$) | $g_u$[e] | TAG[f] | $Q_N$FMT[g] | $Q_N$'[h] | $Q_N$"[i] |
|---|---|---|---|---|---|---|---|---|---|
| 40,567.0170 | 0.0046 | −6.0610 | 3 | 1.5462 | 7 | 62994 | 303 | 3 0 3 | 2 0 2 |
| 40,567.4840 | 0.0047 | −5.1428 | 3 | 1.5462 | 7 | 62994 | 303 | 3 1 3 | 2 0 2 |
| 75,310.2432 | 0.0585 | −4.2732 | 3 | 6.7644 | 13 | 62994 | 303 | 6 0 6 | 5 1 5 |
| 75,310.2432 | 0.0585 | −5.1953 | 3 | 6.7644 | 13 | 62994 | 303 | 6 1 6 | 5 1 5 |
| 75,310.2435 | 0.0585 | −5.1953 | 3 | 6.7644 | 13 | 62994 | 303 | 6 0 6 | 5 0 5 |
| 75,310.2435 | 0.0585 | −4.2732 | 3 | 6.7644 | 13 | 62994 | 303 | 6 1 6 | 5 0 5 |
| 75,338.1091 | 0.0372 | −4.4608 | 3 | 5.9940 | 11 | 62994 | 303 | 5 1 4 | 4 2 3 |
| 75,338.2086 | 0.0372 | −5.3723 | 3 | 5.9940 | 11 | 62994 | 303 | 5 2 4 | 4 2 3 |
| 75,341.3737 | 0.0372 | −5.3722 | 3 | 5.9939 | 11 | 62994 | 303 | 5 1 4 | 4 1 3 |
| 75,341.4732 | 0.0372 | −4.4607 | 3 | 5.9939 | 11 | 62994 | 303 | 5 2 4 | 4 1 3 |

**Notes.**
[a] Estimated or experimental error.
[b] Base 10 logarithm of the integrated intensity at 300 K.
[c] Degrees of freedom in the rotational partition function.
[d] Lower state energy relative to the ground state.
[e] Upper state degeneracy.
[f] Molecular tag or species identifier.
[g] Identifies the format of the quantum numbers.
[h] Quantum numbers for the upper state.
[i] Quantum numbers for the lower state.
(This table is available in its entirety in SPFIT/SPCAT format. A ReadMe is included that describes the contents and how to use it.)

## Appendix B
## Analysis of Acetic Acid toward the G+0.693 Molecular Cloud

To carry out the corresponding LTE analysis of $CH_3COOH$, as well as constrain the excitation conditions, we picked transitions that (i) are not significantly blended with other molecular species and (ii) cover a relatively wide range of rotational energy levels (see Table B1). We employed the set of spectroscopic parameters of the ground vibrational state ($v_t = 0$) of $CH_3COOH$ reported in Ilyushin et al. (2013; entry 60523 of the CDMS catalog; Müller et al. 2005). We again used MADCUBA, leaving as free parameters the molecular column density ($N$), excitation temperature ($T_{ex}$), and radial velocity ($v_{LSR}$). The value of the line width (FWHM) was fixed to 21 km $s^{-1}$ in the fit. In Table 2, we present the derived physical parameters of $CH_3COOH$ along with the physical parameters of formic and carbonic acid, while the results of the LTE fits of the transitions are depicted in Figure 4.

**Table B1**
Spectroscopic Information of the Selected Unblended or Slightly Blended Transitions of $CH_3COOH$ Detected toward G+0.693 (Shown in Figure 4)

| Frequency (GHz) | Transition[a] ($nm^2$ MHz) | log $I$ | $g_u$ ($cm^{-1}$) | $E_{LO}$ (K ) | $E_{up}$ | Comments |
|---|---|---|---|---|---|---|
| 36.7017105 | $3_{0,3}$–$2_{1,2}$ E | −6.6938 | 7 | 1.8 | 4.3 | Unblended |
| 47.6419985 | $4_{1,4}$–$3_{0,3}$ E | −6.3107 | 9 | 3.0 | 6.5 | Unblended |
| 47.7012763 | $4_{1,4}$– $3_{0,3}$ A | −6.3130 | 9 | 2.6 | 6.0 | Blended: $aGg'$–$(CH_2OH)_2$ |
| 78.9564732 | $6_{1,5}$– $5_{2,4}$ A | −5.7912 | 13 | 7.7 | 14.7 | Blended: $HC_7N$ |
| 79.5513516 | $7_{0,7}$– $6_{1,6}$ E | −5.5998 | 15 | 8.8 | 16.4 | Unblended |
| 79.5513690 | $7_{1,7}$– $6_{1,6}$ E | −6.0844 | 15 | 8.8 | 16.4 | Unblended |
| 79.5515061 | $7_{0,7}$– $6_{0,6}$ E | −6.0844 | 15 | 8.8 | 16.4 | Unblended |
| 79.5515235 | $7_{1,7}$– $6_{0,6}$ E | −5.5998 | 15 | 8.8 | 16.4 | Unblended |
| 79.5948832 | $7_{0,7}$– $6_{1,6}$ A | −5.6048 | 15 | 8.4 | 15.9 | Unblended |
| 79.5949136 | $7_{1,7}$– $6_{1,6}$ A | −6.0684 | 15 | 8.4 | 15.9 | Unblended |
| 79.5951321 | $7_{0,7}$– $6_{0,6}$ A | −6.0684 | 15 | 8.4 | 15.9 | Unblended |
| 79.5951625 | $7_{1,7}$– $6_{0,6}$ A | −5.6048 | 15 | 8.4 | 15.9 | Unblended |
| 87.8236760 | $6_{2,4}$– $5_{3,3}$ A | −5.8593 | 13 | 8.8 | 16.8 | Unblended |
| 89.5169537 | $7_{1,6}$– $6_{2,5}$ E | −5.5899 | 15 | 10.6 | 19.5 | Unblended |
| 89.5311839 | $7_{1,6}$– $6_{1,5}$ E | −6.0356 | 15 | 10.6 | 19.5 | Unblended |
| 90.2034364 | $8_{0,8}$– $7_{1,7}$ E | −5.4336 | 17 | 11.5 | 20.7 | Blended: $HCC^{13}C^{13}N$ |
| 90.2034383 | $8_{1,8}$– $7_{1,7}$ E | −5.9223 | 17 | 11.5 | 20.7 | Blended: $HCC^{13}C^{13}N$ |
| 90.2034538 | $8_{0,8}$– $7_{0,7}$ E | −5.9223 | 17 | 11.5 | 20.7 | Blended: $HCC^{13}C^{13}N$ |
| 90.2034556 | $8_{1,8}$– $7_{0,7}$ E | −5.4336 | 17 | 11.5 | 20.7 | Blended: $HCC^{13}C^{13}N$ |
| 90.2462358 | $8_{0,8}$– $7_{1,7}$ A | −5.4378 | 17 | 11.1 | 20.2 | Blended: $CH_3CONH_2$ |
| 90.2462394 | $8_{1,8}$– $7_{1,7}$ A | −5.9027 | 17 | 11.1 | 20.2 | Blended: $CH_3CONH_2$ |
| 90.2462662 | $8_{0,8}$– $7_{0,7}$ A | −5.9027 | 17 | 11.1 | 20.2 | Blended: $CH_3CONH_2$ |
| 90.2462697 | $8_{1,8}$– $7_{0,7}$ A | −5.4378 | 17 | 11.1 | 20.2 | Blended: $CH_3CONH_2$ |
| 100.1687044 | $8_{1,7}$– $7_{2,6}$ E | −5.4228 | 17 | 13.6 | 24.2 | Blended: $CH_3CONH_2$, $HC_4^{13}CN$ and Z-HCCCHNH |
| 100.1689638 | $8_{2,7}$– $7_{2,6}$ E | −5.8783 | 17 | 13.6 | 24.2 | Blended: $CH_3CONH_2$, $HC_4^{13}CN$ and Z-HCCCHNH |
| 100.1706980 | $8_{1,7}$– $7_{1,6}$ E | −5.8783 | 17 | 13.6 | 24.2 | Blended: $CH_3CONH_2$, $HC_4^{13}CN$ |
| 100.1709574 | $8_{2,7}$– $7_{1,6}$ E | −5.4228 | 17 | 13.6 | 24.2 | Blended: $CH_3CONH_2$, $HC_4^{13}CN$ |
| 100.8554272 | $9_{0,9}$– $8_{1,8}$ E | −5.2883 | 19 | 14.5 | 25.5 | Blended: $CH_3NCHO$ and U-line |
| 100.8554274 | $9_{1,9}$– $8_{1,8}$ E | −5.7817 | 19 | 14.5 | 25.5 | Blended: $CH_3NCHO$ and U-line |
| 100.8554291 | $9_{0,9}$– $8_{0,8}$ E | −5.7817 | 19 | 14.5 | 25.5 | Blended: $CH_3NCHO$ and U-line |
| 100.8554293 | $9_{1,9}$– $8_{0,8}$ E | −5.2883 | 19 | 14.5 | 25.5 | Blended: $CH_3NCHO$ and U-line |
| 100.8974541 | $9_{0,9}$– $8_{1,8}$ A | −5.2943 | 19 | 14.1 | 25.0 | Unblended |
| 100.8974545 | $9_{1,9}$– $8_{1,8}$ A | −5.7585 | 19 | 14.1 | 25.0 | Unblended |
| 100.8974577 | $9_{0,9}$– $8_{0,8}$ A | −5.7585 | 19 | 14.1 | 25.0 | Unblended |
| 100.8974581 | $9_{1,9}$– $8_{0,8}$ A | −5.2943 | 19 | 14.1 | 25.0 | Unblended |
| 111.0975729 | $5_{5,0}$– $4_{1,1}$ A | −5.5160 | 11 | 7.2 | 15.5 | Blended: $aGg'$–$(CH_2OH)_2$ |
| 111.5072803 | $10_{0,10}$–$9_{1,9}$ E | −5.1575 | 21 | 17.8 | 30.8 | Unblended |
| 111.5072803 | $10_{1,10}$–$9_{1,9}$ E | −5.6580 | 21 | 17.8 | 30.8 | Unblended |
| 111.5072805 | $10_{1,10}$–$9_{0,9}$ E | −5.1575 | 21 | 17.8 | 30.8 | Unblended |
| 111.5072805 | $10_{0,10}$–$9_{0,9}$ E | −5.6580 | 21 | 17.8 | 30.8 | Unblended |
| 111.5485353 | $10_{0,10}$–$9_{1,9}$ A | −5.1649 | 21 | 17.5 | 30.3 | Blended: $CH_3C_3N$ |
| 111.5485353 | $10_{1,10}$–$9_{1,9}$ A | −5.6307 | 21 | 17.5 | 30.3 | Blended: $CH_3C_3N$ |
| 111.5485357 | $10_{1,10}$–$9_{0,9}$ A | −5.1649 | 21 | 17.5 | 30.3 | Blended: $CH_3C_3N$ |
| 111.5485357 | $10_{0,10}$–$9_{0,9}$ A | −5.6307 | 21 | 17.5 | 30.3 | Blended: $CH_3C_3N$ |
| 154.3545087 | $7_{7,1}$– $6_{6,1}$ E | −5.0690 | 15 | 15.4 | 29.3 | Unblended |

**Note.**
[a] The rotational energy levels are labeled using the conventional notation for asymmetric tops, $J_{K_a,K_c}$, where $J$ denotes the angular momentum quantum number, and $K_a$ and $K_c$ are projections of $J$ along the $a$ and $c$ principal axes. The $A$ and $E$ labels refer to the $A$ and $E$ substates, respectively, originated from the methyl internal rotation molecule.

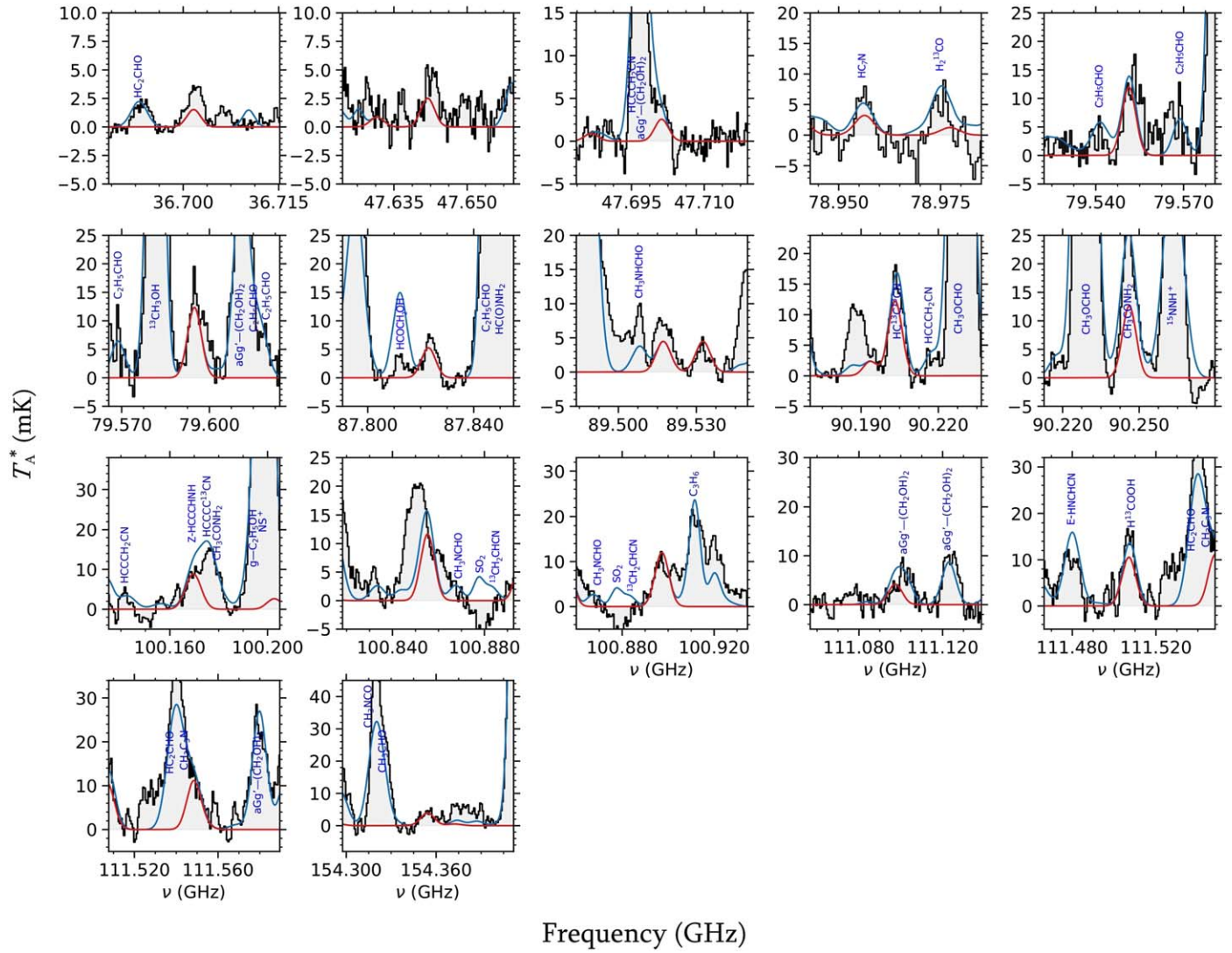


**Figure 4.** Selected transitions of $CH_3COOH$ identified toward the G+0.693 molecular cloud. The best LTE fit computed with MADCUBA-SLIM is depicted as a red solid line, and the predicted molecular emission from all of the molecules identified in our spectral survey is shown in blue (observed spectra plotted as gray histograms).

## Appendix C
## Tentative Detection of *cis*-HCOOH toward G+0.693

We employed the rotational data of the ground vibrational state of *c*-HCOOH reported in Winnewisser et al. (2002), which corresponds to entry 046507 of the CDMS catalog (Müller et al. 2005). We have detected three lines with negligible contamination from other species and five additional lines exhibiting slight blends, although the overall detection of this conformer is somewhat tentative (see Table C1). Nevertheless, many other lines that are also predicted to be very bright (e.g., the $5_{0,5}$–$4_{0,4}$ and $2_{0,2}$–$1_{0,1}$ transitions) could not be included in the current analysis because they are significantly blended with other molecular species. We thus used MADCUBA-SLIM, in this case leaving as free parameters the molecular column density ($N$) and line width (FWHM), while the value of the excitation temperature ($T_{ex}$) and radial velocity ($v_{LSR}$) were fixed in the fit to the values of *t*-HCOOH (Rodríguez-Almeida et al. 2021a). The derived physical parameters of *c*-HCOOH are listed in Table 2, and the results of the LTE fits of the lines are shown in Figure 5.

**Table C1**
Spectroscopic Information of the Selected Unblended or Slightly Blended Transitions of *c*-HCOOH Detected toward G+0.693 (Shown in Figure 5)

| Frequency (GHz) | Transition[a] | log $I$ ($nm^2$ MHz) | $g_u$ | $E_{LO}$ ($cm^{-1}$) | $E_{up}$ (K ) | Comments |
|---|---|---|---|---|---|---|
| 45.3513500 | $2_{1,1}-1_{1,0}$ | −4.7855 | 5 | 3.3 | 6.8 | Unblended |
| 76.1753218 | $1_{1,0}-1_{0,1}$ | −4.3110 | 3 | 0.7 | 4.7 | Blended with $CH_3NHCHO$ |
| 77.6001999 | $2_{1,1}-2_{0,2}$ | −4.0803 | 5 | 2.2 | 6.8 | Blended with $H_2CCCHCN$ |
| 85.0427471 | $4_{1,4}-3_{1,3}$ | −3.8501 | 9 | 6.8 | 13.7 | Unblended |
| 87.6946938 | $4_{0,4}-3_{0,3}$ | −3.7907 | 9 | 4.4 | 10.5 | Blended with $CH_3CONH_2$ and U-line |
| 106.2665926 | $5_{1,5}-4_{1,4}$ | −3.5561 | 11 | 9.6 | 18.8 | Blended with *Aa*-$CH_3CH_2CH_2OH$ |
| 131.1498866 | $6_{0,6}-5_{0,5}$ | −3.2804 | 13 | 11.0 | 21.9 | Unblended |
| 137.1847188 | $3_{1,3}-2_{0,2}$ | −3.6782 | 7 | 2.2 | 9.7 | Blended with $SiC_2$ |

**Note.**
[a] The rotational energy levels are labeled using the conventional notation for asymmetric tops, $J_{K_a,K_c}$, where $J$ denotes the angular momentum quantum number, and $K_a$ and $K_c$ are projections of $J$ along the $a$ and $c$ principal axes.

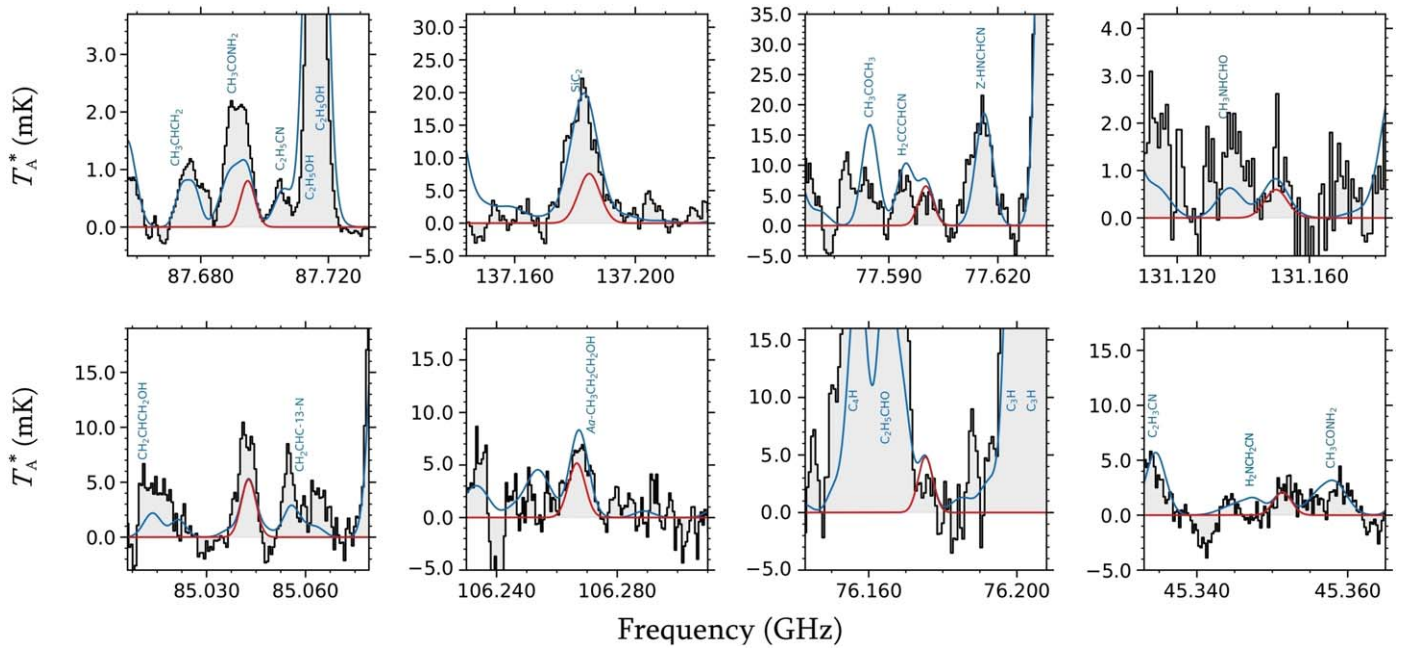


**Figure 5.** Selected transitions of *c*-HCOOH identified toward the G+0.693 molecular cloud. The best LTE fit computed with MADCUBA is depicted as a red solid line, while the expected molecular emission from all of the molecular species identified in our spectral survey is shown in blue (observed spectra plotted as gray histograms).

## Appendix D
## Complementary Figures

In Figure 6, we provide a visual comparison of the abundance ratio between HCOOH and $CH_3COOH$ toward different astronomical environments.

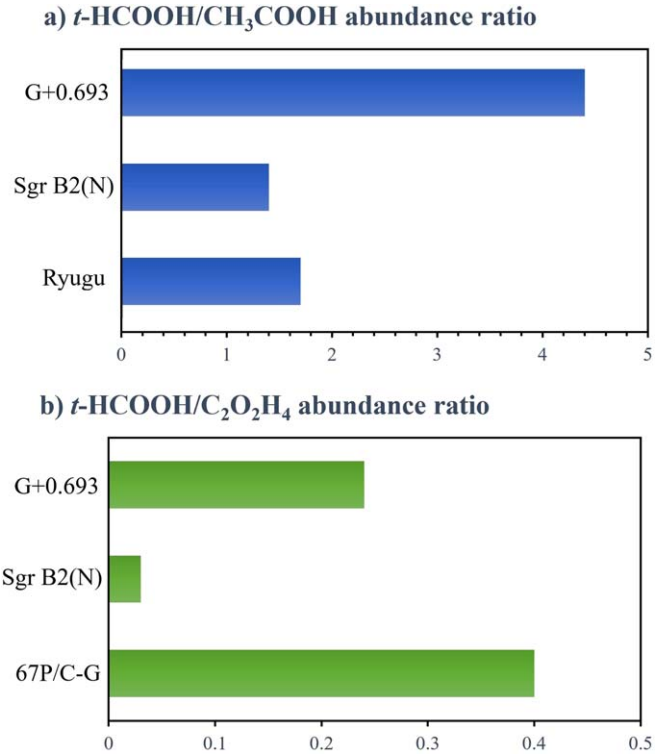


**Figure 6.** Abundance ratio between formic and acetic acid toward different astronomical environments

## ORCID iDs

Miguel Sanz-Novo https://orcid.org/0000-0001-9629-0257
Víctor M. Rivilla https://orcid.org/0000-0002-2887-5859
Izaskun Jiménez-Serra https://orcid.org/0000-0003-4493-8714
Jesús Martín-Pintado https://orcid.org/0000-0003-4561-3508
Laura Colzi https://orcid.org/0000-0001-8064-6394
Shaoshan Zeng https://orcid.org/0000-0003-3721-374X
Andrés Megías https://orcid.org/0000-0002-6389-7172
Álvaro López-Gallifa https://orcid.org/0000-0001-6049-9366
Antonio Martínez-Henares https://orcid.org/0000-0001-5191-2075
Sarah Massalkhi https://orcid.org/0000-0002-7387-9787
Belén Tercero https://orcid.org/0000-0002-4782-5259
Pablo de Vicente https://orcid.org/0000-0002-5902-5005
Sergio Martín https://orcid.org/0000-0001-9281-2919
David San Andrés https://orcid.org/0000-0001-7535-4397
Miguel A. Requena-Torres https://orcid.org/0009-0009-5346-7329

## References

Adamczyk, K., Prémont-Schwarz, M., Pines, D., Pines, E., & Nibbering, E. T. J. 2009, Sci, 326, 1690
Agúndez, M., Marcelino, N., Cernicharo, J., Roueff, E., & Tafalla, M. 2019, A&A, 625, A147
Alonso, E. R., Kolesniková, L., Peña, I., et al. 2015, JMoSp, 316, 84
Altwegg, K., Balsiger, H., Bar-Nun, A., et al. 2016, SciA, 2, e1600285
Altwegg, K., Balsiger, H., Bar-Nun, A., et al. 2016, SciA, 2, e1600285
Armijos-Abendaño, J., Martín-Pintado, J., Requena-Torres, M. A., Martín, S., & Rodríguez-Franco, A. 2015, MNRAS, 446, 3842
Baltrusaitis, J., & Grassian, V. H. 2010, JPCA, 114, 2350
Belloche, A., Müller, H. S. P., Menten, K. M., Schilke, P., & Comito, C. 2013, A&A, 559, A47
Bennett, C. J., Ennis, C. P., & Kaiser, R. I. 2014, ApJ, 794, 57
Blom, C. E., & Bauder, A. 1981, CPL, 82, 492
Caldeira, K., & Wickett, E. M. E. 2003, Natur, 425, 365
Combes, F., Q-Rieu, N., & Wlodarczak, G. 1996, A&A, 308, 618
Cooper, G. W., Onwo, W. M., & Cronin, J. R. 1992, GeCoA, 56, 4109
Cuadrado, S., Goicoechea, J. R., Roncero, O., et al. 2016, A&A, 596, L1
Cunningham, M. R., Jones, P. A., Godfrey, P. D., et al. 2007, MNRAS, 376, 1201
Delitsky, M. L., & Lane, A. L. 1998, JGR, 103, 31391
Delitsky, M. L., Paige, D. A., Siegler, M. A., et al. 2017, Icar, 281, 19
Drozdovskaya, M. N. 2019, From Stars to Planets II—Connecting our Understanding of Star and Planet Formation, 5
Ehrenfreund, P., Bernstein, M. P., Dworkin, J. P., Sandford, S. A., & Allamandola, L. J. 2001, ApJL, 550, L95
García de la Concepción, J., Colzi, L., Jiménez-Serra, I., et al. 2022, A&A, 658, A150
García de la Concepción, J., Jiménez-Serra, I., Carlos Corchado, J., Rivilla, V. M., & Martín-Pintado, J. 2021, ApJL, 912, L6
Georgiou, C. D., & Deamer, D. W. 2014, AsBio, 14, 541
Gerakines, P. A., Moore, M. H., & Hudson, R. L. 2000, A&A, 357, 793
Ghoshal, S., & Hazra, M. K. 2015, RSCAd, 5, 17623
Glavin, D. P., Callahan, M. P., Dworkin, J. P., & Elsila, J. E. 2010, M&PS, 45, 1948
Goldsmith, P. F., & Langer, W. D. 1999, ApJ, 517, 209
Gordy, W., & Cook, R. L. 1984, Microwave Molecular Spectra (3rd ed.; New York: Wiley)
Hage, W., Liedl, K. R., Hallbrucker, A., & Mayer, E. 1998, Sci, 279, 1332
Herbst, E., Gianfranco, V., & Ceccarelli, C. 2020, ESC, 4, 488
Hollis, J. M., Pedelty, J. A., Snyder, L. E., et al. 2003, ApJ, 588, 353
Ilyushin, V. V., Endres, C. P., Lewen, F., Schlemmer, S., & Drouin, B. J. 2013, JMoSp, 290, 31
Ilyushin, V. V., Margulès, L., Tercero, B., et al. 2021, JMoSp, 379, 111454
Ioppolo, S., Kaňuchová, Z., James, R. L., et al. 2021, A&A, 646, A172
Irvine, W. M., Friberg, P., Kaifu, N., et al. 1990, A&A, 229, L9
Jiménez-Serra, I., Martín-Pintado, J., Rivilla, V. M., et al. 2020, AsBio, 20, 1048
Jimenez-Serra, I., Rodriguez-Almeida, L. F., Martin-Pintado, J., et al. 2022, A&A, 663, A181
Jiménez-Serra, I., Vasyunin, A. I., Caselli, P., et al. 2016, ApJL, 830, L6
Jones, B. M., Kaiser, R. I., & Strazzulla, G. 2014, ApJ, 788, 170
Jones, P. A., Cunningham, M. R., Godfrey, P. D., & Cragg, D. M. 2007, MNRAS, 374, 579
Jørgensen, J. K., Müller, H. S. P., Calcutt, H., et al. 2018, A&A, 620, A170
Kolesniková, L., León, I., Alonso, E. R., Mata, S., & Alonso, J. L. 2019, J. Phys. Chem. Lett., 10, 1325
Kuan, Y.-J., Charnley, S. B., Huang, H.-C., Tseng, W.-L., & Kisiel, Z. 2003, ApJ, 593, 848
Lefloch, B., Ceccarelli, C., Codella, C., et al. 2017, MNRAS Lett., 469, L73
Lester, M. I., Pond, B. V., Marshall, M. D., et al. 2001, FaDi, 118, 373
Liu, S.-Y., Girart, J. M., Remijan, A., & Snyder, L. E. 2002, ApJ, 576, 255
Loerting, T., Tautermann, C., Kroemer, R., et al. 2000, Angew. Chem. Int. Ed., 39, 5
Maçôas, E. M. S., Khriachtchev, L., Pettersson, M., Fausto, R., & Räsänen, M. 2005, PCCP, 7, 743
Majumdar, L., Gratier, P., Wakelam, V., et al. 2018, MNRAS, 477, 525
Markmeyer, M. N., Lamberts, T., Meisner, J., & Kästner, J. 2019, MNRAS, 482, 293
Martín, S., Martín-Pintado, J., Blanco-Sánchez, C., et al. 2019, A&A, 631, A159
Martín, S., Requena-Torres, M. A., Martín-Pintado, J., & Mauersberger, R. 2008, ApJ, 678, 245
McGuire, B. A. 2022, ApJS, 259, 30
Megías, A., Jiménez-Serra, I., Martín-Pintado, J., et al. 2023, MNRAS, 519, 1601
Mehringer, D. M., Snyder, L. E., Miao, Y., & Lovas, F. J. 1997, ApJL, 480, L71
Molpeceres, G., Jiménez-Serra, I., Oba, Y., et al. 2022, A&A, 663, A41
Molpeceres, G., & Rivilla, V. M. 2022, A&A, 665, A27
Moore, M. H., Hudson, R. L., & Gerakines, P. A. 2001, AcSpA, 57, 843
Mori, T., Suma, K., Sumiyoshi, Y., & Endo, Y. 2009, JChPh, 130, 204308
Mori, T., Suma, K., Sumiyoshi, Y., & Endo, Y. 2011, JChPh, 134, 044319
Müller, H. S. P., Schlöder, F., Stutzki, J., & Winnewisser, G. 2005, JMoSt, 742, 215
Naraoka, H., Takano, Y., Dworkin, J. P., Yasuhiro, O., & Hamase, K. 2023, Sci, 379, abn9033
Nguyen, T. L., Xue, B. C., Weston, R. E. J., Barker, J. R., & Stanton, J. F. 2012, J. Phys. Chem. Lett., 3, 1549

Noble, J. A., Dulieu, F., Congiu, E., & Fraser, H. J. 2011, ApJ, 735, 121
Oba, Y., Watanabe, N., Kouchi, A., Hama, T., & Pirronello, V. 2010, ApJ, 722, 1598
Pettersson, M., Maçôas, E. M. S., Khriachtchev, L., et al. 2002, JChPh, 117, 9095
Pickett, H. M. 1991, JMoSp, 148, 371
Pickett, H. M., Poynter, R. L., Cohen, E. A., et al. 1998, JQSRT, 60, 883
Pizzarello, S., Schrader, D. L., Monroe, A. A., & Lauretta, D. S. 2012, PNAS, 109, 11949
Pizzarello, S., & Shock, E. 2010, Cold Spring Harbor Perspectives in Biology, 2, 3
Qasim, D., Lamberts, T., He, J., et al. 2019, A&A, 626, A118
Remijan, A., Snyder, L. E., Friedel, D. N., Liu, S.-Y., & Shah, R. Y. 2003, ApJ, 590, 314
Requena-Torres, M. A., Martín-Pintado, J., Martín, S., & Morris, M. R. 2008, ApJ, 672, 352
Requena-Torres, M. A., Martín-Pintado, J., Rodríguez-Franco, A., et al. 2006, A&A, 455, 971
Rivilla, V. M., Beltrán, M. T., Martín-Pintado, J., et al. 2017, A&A, 599, A26
Rivilla, V. M., Colzi, L., Jiménez-Serra, I., et al. 2022a, ApJL, 929, L11
Rivilla, V. M., García de la Concepción, J., Jiménez-Serra, I., et al. 2022b, FrASS, 9, 829288
Rivilla, V. M., Jiménez-Serra, I., García de la Concepción, J., et al. 2021b, MNRAS, 506, L79
Rivilla, V. M., Jiménez-Serra, I., Martín-Pintado, J., et al. 2021a, PNAS, 118, e2101314118
Rivilla, V. M., Martín-Pintado, J., Jiménez-Serra, I., et al. 2019, MNRAS, 483, L114
Rivilla, V. M., Martín-Pintado, J., Jiménez-Serra, I., et al. 2020, ApJL, 899, L28
Rodríguez-Almeida, L. F., Jiménez-Serra, I., Rivilla, V. M., et al. 2021a, ApJL, 912, L11
Rodríguez-Almeida, L. F., Rivilla, V. M., Jiménez-Serra, I., et al. 2021b, A&A, 654, L1
Ruaud, M., Loison, J. C., Hickson, K. M., et al. 2015, MNRAS, 447, 4004
Rubin, M., Bekaert, D. V., Broadley, M. W., Drozdovskaya, M. N., & Wampfler, S. F. 2019, ESC, 3, 1792
Sanz-Novo, M., León, I., Alonso, E. R., Kolesniková, L., & Alonso, J. L. 2021, ApJ, 915, 76
Sephton, M. A. 2002, NPRep, 19, 292
Snyder, L. E., Lovas, F. J., Hollis, J. M., et al. 2005, ApJ, 619, 914
Strazzulla, G., Brucato, J. R., Cimino, G., & Palumbo, M. E. 1996, P&SS, 44, 1447
Tachikawa, H., & Kawabata, H. 2016, JPCA, 120, 6596
Taquet, V., Wirström, E. S., Charnley, S. B., et al. 2017, A&A, 607, A20
Tercero, B., Cuadrado, S., López, A., et al. 2018, A&A, 620, L6
Tercero, F., López-Pérez, J. A., Gallego, J. D., et al. 2021, A&A, 645, A37
Thaddeus, P., Guelin, M., & Linke, R. A. 1981, ApJL, 246, L41
Tsuge, M., & Khriachtchev, L. 2015, JPCA, 119, 2628
Wagner, J. P., Reisenauer, H. P., Hirvonen, V., et al. 2016, Chem. Commun., 52, 7858
Wang, H., Zeuschner, J., Eremets, M., Troyan, I., & Willams, J. 2016, NatSR, 6, 19902
Winnewisser, M., Winnewisser, B. P., Stein, M., et al. 2002, JMoSp, 216, 259
Zeng, S., Jiménez-Serra, I., Rivilla, V. M., et al. 2018, MNRAS, 478, 2962
Zeng, S., Jiménez-Serra, I., Rivilla, V. M., et al. 2021, ApJL, 920, L27
Zeng, S., Rivilla, V. M., Jiménez-Serra, I., et al. 2023, MNRAS, 523, 1448
Zeng, S., Zhang, Q., Jiménez-Serra, I., et al. 2020, MNRAS, 497, 4896
Zheng, W., & Kaiser, R. I. 2007, CPL, 450, 55
Zhu, C., Turner, A. M., Abplanalp, M. J., & Kaiser, R. I. 2018, ApJS, 234, 15
Zuckerman, B., Ball, J. A., & Gottlieb, C. A. 1971, ApJ, 163, L41